Discover Nano

Research

Development of blue-light GaN based micro light-emitting diodes using ion implantation technology

Yu-Hsuan Hsu[1,2] · Shao-Hua Lin[1] · Dong-Sing Wuu[3] · Ray-Hua Horng[2]

Received: 21 September 2024 / Accepted: 9 December 2024
Published online: 18 December 2024

Abstract
This study fabricated 10 μm chip size μLEDs of blue-light GaN based epilayers structure with different mesa processes using dry etching and ion implantation technology. Two ion sources, As and Ar, were applied to implant into the LED structure to achieve material isolation and avoid defects on the mesa sidewall caused by the plasma process. Excellent turn-on behavior was obtained in both ion-implanted samples, which also exhibited lower leakage current compared to the sample fabricated by the dry etching process. Additionally, lower dynamic resistance (R_d) and series resistance (R_s) were obtained with Ar implantation, leading to a better wall-plug efficiency of 10.66% in this sample. Consequently, outstanding external quantum efficiency (EQE) values were also present in both implant samples, particularly in the sample implanted with Ar ions. This study proves that reducing defects on the mesa sidewall can further enhance device properties by suppressing non-radiative recombination behavior in small chip size devices. Overall, if implantation is used to replace the traditional dry etching process for mesa fabrication, the ideality factor can decrease from 11.89 to 2.2, and EQE can improve from 8.67 to 11.03%.

Keywords Micro-LED · Dry etching · Ion implantation · Wall-plug efficiency

1 Introduction

In recent years, the field of optoelectronics has witnessed a remarkable surge in interest and innovation, driven by the quest for more efficient, compact, and versatile lighting and display technologies. Among these, micro light emitting diodes (μLEDs) have emerged as a promising solution, offering unprecedented levels of miniaturization, energy efficiency, and performance. μLEDs have garnered significant interest due to their numerous advantages, including high luminous intensity, resolution, contrast, response speed, lifespan, and energy efficiency [1–4]. Recognized for these exceptional performance characteristics, μLEDs are considered at the forefront of next-generation display technology. They find applications across various domains, from wearable devices like wristbands and watches to large-scale commercial billboards, public displays, and immersive technologies such as virtual reality (VR) or augmented reality (AR) devices [5–7]. However, as device dimensions shrink to the microscale, the influence of sidewall effects and non-radiative recombination becomes increasingly pronounced [8, 9]. Sidewall effects refer to the interaction between carriers and sidewall surfaces in μLEDs, leading to non-uniform carrier distribution, enhanced surface recombination, and reduced device efficiency. Non-radiative recombination processes involve the generation of electron–hole pairs that do not contribute

✉ Ray-Hua Horng, rayhua@nycu.edu.tw | [1]Institute of Electronics, National Yang Ming Chiao Tung University, Hsinchu 30010, Taiwan, ROC. [2]Department of Photonics, National Yang Ming Chiao Tung University, Hsinchu 30010, Taiwan, ROC. [3]Department of Applied Materials and Optoelectronic Engineering, National Chi Nan University, Nantou 54561, Taiwan, ROC.

to light emission, leading to wasted energy and decreased quantum efficiency [10]. Understanding and mitigating these phenomena are critical for optimizing the performance and reliability of μLED devices. In μLEDs, the high surface-to-volume ratio exacerbates sidewall effects, causing deviations from ideal device behavior [11, 12]. As carriers approach the sidewall surfaces, they experience surface recombination and scattering, leading to non-uniform carrier distribution and reduced injection efficiency. Moreover, sidewall roughness and defects can trap carriers, increasing the likelihood of non-radiative recombination and reducing light output [7, 8, 13]. Experimental studies have revealed the detrimental impact of sidewall effects on device performance, highlighting the need for strategies to minimize sidewall-related losses. Suppressing sidewall damage is a critical challenge in μLEDs fabrication, as defects introduced during the etching process can lead to leakage currents, reduced efficiency, and poor device reliability. Various methods have been developed to address this issue, such as plasma treatments using gases such as oxygen, hydrogen, and nitrogen form protective passivation layers, wet chemical treatments like KOH etching or sulfur passivation remove damage layers and improve surface quality [14, 15]. Atomic layer deposition (ALD) further contributes by depositing conformal passivation layers, such as Al_2O_3, which protect against leakage currents and enhance optical performance [8]. Novel etching technique, such as neutral beam etching, minimized defect generation during fabrication [16]. Furthermore, ion implantation, particularly with the careful selection of ion implantation elements, researchers can effectively suppress sidewall damage and improve the performance and reliability of microLED devices.

Ion implantation is a crucial process used in semiconductor manufacturing to introduce impurities into a substrate, altering its electrical properties. In microLED fabrication, ion implantation is a critical process for passivating defects and mitigating sidewall damage, improving device efficiency and reliability [17–25]. Various elements have been employed, each offering unique advantages. Fluorine is widely used for its ability to effectively passivate dangling bonds, reducing non-radiative recombination and leakage currents [22]. Nitrogen is particularly effective in GaN-based microLEDs, where it chemically bonds with the material to stabilize the surface and suppress recombination. Hydrogen is highly effective in forming stable complexes with defects, significantly reducing non-radiative recombination, although its thermal stability requires careful management [19]. The heavy ions, such as Ar, Kr, Xe, and As of different implantation energies and dosages have be demonstrated to play the isolation function and confine non-radiative regions to produce relatively invariant luminance in μLEDs display [19]. By carefully selecting these elements based on specific fabrication needs, ion implantation can significantly enhance the performance and reliability of microLED devices. A study to optimize implant energy for the mesa process in μLED fabrication, specifically targeting a 50 μm chip size has been studied using heavy ion ^{75}As in our group [26]. The heavy ion ^{75}As was employed to disrupt the crystal structure in the LED epilayer, facilitating isolation. Through electrical measurements, we determined that 40 keV is the optimal implant energy for achieving a mesa depth of 700 nm. Furthermore, our investigation revealed that a gradual energy implantation process results in a lower forward voltage at 1 mA, and multi-energies implantation leads to higher light emission intensity. Consequently, we introduced another ion source, ^{40}Ar, for comparison with ^{75}As ions. Additionally, μLED is also fabricated using the traditional ICPRIE process, serving as control samples for comparision. The chip sizes were reduced to 10 μm in this study, enabling clearer observation of the non-radiative effect.

2 Experimental

The commercial InGaN/GaN blue light LED epilayer structure was grown on a 4-inch sapphire substrate, comprising a 100 nm-thick layer of indium-tin oxide (ITO) deposited by E-gun evaporation system at 270 °C, a 400 nm-thick layer of p-GaN, 300 nm-thick multiple quantum wells (MQWs), and a 4 μm-thick layer of n-GaN. To establish Ohmic contact between ITO and p-GaN, an annealing process was conducted at 500 °C in air ambient after depositing ITO layer. Two process flows were carried out in this study, including ion implantation and dry etching by inductive coupled plasma reactive ion etching (ICPRIE) to perform the mesa process. For the implantation process, the process flow was schematically illustrated in Fig. 1a–e. Initially, the ITO layer with photoreisit mask was etched using an HCl-$FeCl_3$ solution to define the emission area in the μLED array, as depicted in Fig. 1a. Subsequently, ion implantation was employed to isolate each pixel using the photoreisit mask, depicted in Fig. 1b. To expose the n-GaN, the n-side region with photoreisit mask was etched using ICPRIE, illustrated in Fig. 1c, followed by redeposition of ITO to connect the p-side pixels, as shown in Fig. 1d. Finally, the n and p metals (Ti/Al 40 nm/400 nm) were simultaneously deposited on the contact pad areas to be n and p electrodes, as depicted in Fig. 1e. For the fabrication of traditional LEDs using ICPRIE, the process flow was presented in Fig. 1f, i. Similar to the implantation process, defining emission patterns using the photoresist was achieved by etching ITO and performing the mesa process using ICPRIE dry etching, as

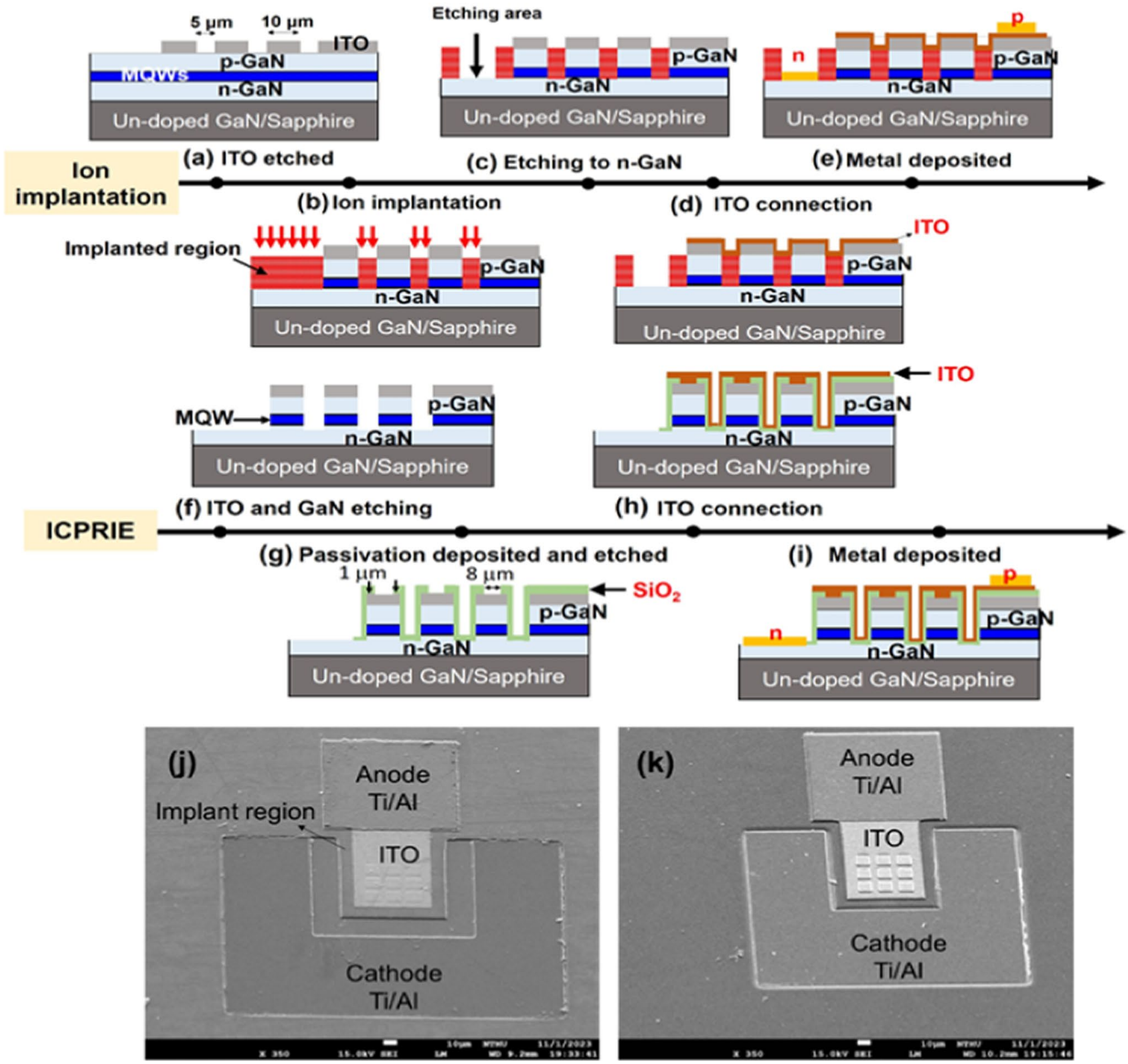

Fig. 1 Ion implant process flow for **a** ITO etched, **b** ion implantation, **c** etching to n-GaN, **d** ITO connection, **e** metal deposited, and the ICPRIE process flow for **f** ITO and GaN etched, **g** passivation deposited, **h** ITO connection, **i** metal deposited, the SEM picture for **j** implantation and **k** ICPRIE process samples

shown in Fig. 1f. Subsequently, to connect the p-side pixels, a passivation layer was deposited by plasma-enhanced chemical vapor deposition (PECVD) before depositing the common ITO electrode, as illustrated in Fig. 1g. The 500-nm thick SiO_2 layer was etched using ICPRIE dry etching. Note that, although the chip size was 10 um and design for top emission, the passivation was used to cover the sidewalls and partial top area, which prevented from leakage for the ICPRIE samples. The edge region was about 1 um. Next, the common ITO layer was deposited on each pixel, as shown in Fig. 1h, followed by deposition of both p and n metals using E-beam evaporation system, as depicted in Fig. 1i. Figure 1j, k present the top-view images of the final μLED arrays fabricated using ion implantation and ICPRIE processes, respectively, observed by scanning electron microscope (SEM). The μLED array featured a $10 \times 10\ \mu m^2$ chip size with 15 μm pitch and a 3×3 array pattern.

In this study, stopping and range of ions in matter (SRIM) software was utilized to simulate the ion distribution of depth after the implantation process. The target substrate selected was GaN with a material density of 6.15 g/cm^3. The

Table 1 Ion implantation parameters of ^{75}As and ^{40}Ar ions in this study

Samples	Ion	Total dosage (cm^{-2})	Implant energy (keV)
μLED (As)	^{75}As	4×10^{14}	40→30→20→10
μLED (Ar)	^{40}Ar	8×10^{14}	40→15→10

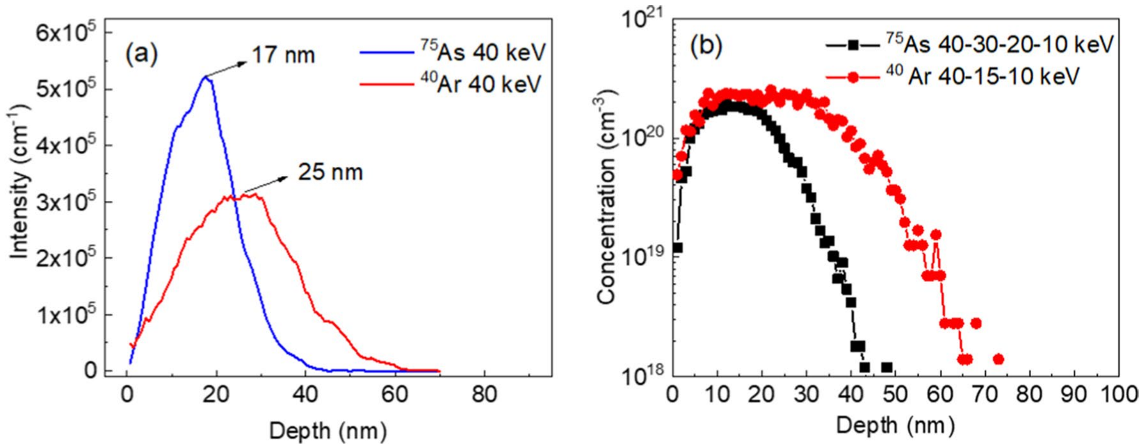

Fig. 2 Ion distributions of ^{75}As, and ^{40}Ar with **a** 40 keV and **b** 40–10 keV implantation energy by SRIM simulation

implant energy was optimized in our previous study, where the mesa process in μLED fabrication using 40 keV was found suitable for isolating each pixel using the heavy ion ^{75}As. Considering the two ion species, ^{75}As and ^{40}Ar, with different masses, the ion distribution was adjusted by dosage using SRIM software. Ion implantation parameters are listed in Table 1. Since the mass of ^{40}Ar is less than that of ^{75}As, the total dosage was fixed at twice the amount for ^{40}Ar compared to ^{75}As. Therefore, total dosages were set at 4×10^{14} and 8×10^{14} for ^{75}As and ^{40}Ar ions, respectively. To compare with the implantation process, a μLED array was also fabricated by ICPRIE as the control sample, referred to as μLED (ICP) in this study. Electrical characteristics of the μLEDs were measured using an Agilent 4155B semiconductor parameter analyzer. Subsequently, a charge-coupled device (CCD) was employed to observe the corresponding emission pattern, and light intensity profiles were analyzed using ImageJ software for both implant and ICPRIE processes. The optoelectrical properties were measured using a multi-function power meter KEITHLEY 2400 with integrating sphere systems.

3 Results and discussion

In our previous study, we found that implanting energy at 40 keV using ^{75}As ions can effectively reach the depth required for the mesa process. Figure 2a illustrates the ion distribution of two ions ^{75}As and ^{40}Ar with a 40 keV implant energy, as simulated using SRIM. It's well-known that higher atomic mass can induce more damage to the material but tends to halt at shallower depths. Due to the differing atomic masses of ^{75}As and ^{40}Ar, the peak of ion distribution occurs at 25 nm for ^{40}Ar and at 17 nm for ^{75}As at the same implant energy. Based the result, we adjusted the implant dosage to compare the effects of these two ion sources, as simulating the exact damage situation with SRIM can be challenging. Since ^{75}As has nearly twice the atomic mass of ^{40}Ar, we set the total dosage at 4×10^{14} and 8×10^{14} for ^{75}As and ^{40}Ar, respectively. These values were chosen to ensure a fair comparison between the two ion sources. Additionally, Table 1 listed the implantation energies utilized in our study. We employed a gradient method, implanting from high to low energy, to extend the implant distance into deeper regions, leveraging the channel tunneling effect. To avoid the generation of leakage carriers from the shallow area, the implant energies were adjusted using SRIM to achieve a square-shaped ion concentration profile. The parameters of implantation were thoroughly simulated using SRIM, as depicted in Fig. 2b.

A sample fabricated using ICPRIE for the mesa process was also prepared to compare with the implant samples. The forward current as function of voltage (I-V) ranging from 2.0 to 4.0 V was presented in Fig. 3a. The highest slope of the I-V curve, observed between 3.0 to 3.5 V, was obtained in the μLED (Ar) sample. Specifically, the currents measured at 3 V were 0.97 mA, 1.14 mA, and 0.90 mA for the μLED (As), μLED (Ar), and μLED (ICP) samples, respectively. This suggests that μLED (Ar) exhibited the lowest dynamic resistance (R_d) at 3 V, as detailed in Table 2, presenting the best electrical performance among

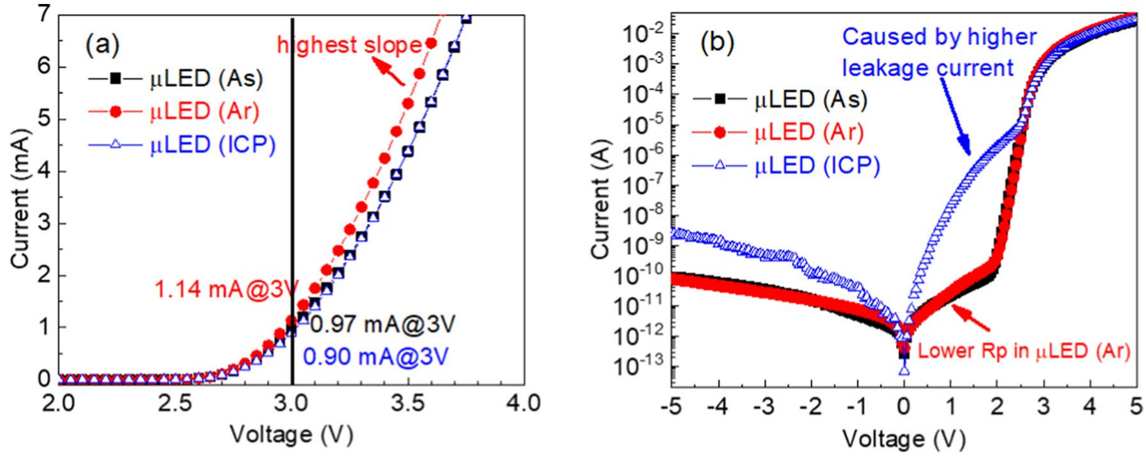

Fig. 3 The I-V curves of three samples **a** from 2 to 4 V with linear scale, and **b** from − 5 to 5 V in log scale

the three samples. Furthermore, the series resistance (R_s) between 3 to 4 V was found to be 109.2 Ω for μLED (As), 89.4 Ω for μLED (Ar), and 108.6 Ω for μLED (ICPRIE). The higher R_s observed in μLED (ICPRIE) may be attributed to the disappointing carrier input efficiency caused by increased leakage current, where many carriers flow into the sidewall and become trapped by the dangling bonds on the mesa sidewall. Similarly, a higher Rs was also observed in μLED (As) compared to μLED (Ar), potentially due to damage in the n-GaN layer, further resulting to higher R_s in μLED (As). To delve deeper into these results, the log scale of the IV curve was also plotted in Fig. 3b, providing a clearer view of the electrical properties. From Fig. 3b, it can be observed that the μLED (ICP) sample exhibited significant leakage issues and early turn-on problems. The leakage current (2.6 μA @ − 5 V) of μLED (ICP) was more than one order of magnitude higher than that of both implantation samples, which displayed lower leakage currents (1 nA @ − 5 V). Although the passivation has covered the sidewalls and partial top area (described at the Experimental section), obviously, the passivation did not be effective for the ICPRIE samples. This result suggested that the electrical properties were enhanced by avoiding the creation of a sidewall in μLED devices. Moreover, a lower parallel resistance (R_p) was observed in μLED (^{40}Ar) compared to μLED (^{75}As). In μLED devices, R_p represents the leakage current before the device turns on, with values listed in Table 2 as 20.7 GΩ for μLED (^{75}As) and 11.7 GΩ for μLED (Ar) from 0.5 to 1.5 V. A higher R_p indicated less leakage carrier flow from the anode to cathode, implying a better isolation effect. Compared to μLED (^{40}Ar), although a lower implantation dosage was applied in μLED (As), the heavier ions can cause more significant damage to the crystal structure, resulting in a better isolation process in the semiconductor material. Moreover, the most important indicative values, considered as an ideality factor, were also calculated and fitted within the turn-on region from 2 to 2.3 V, as listed in Table 2. Clearly, the ideality factor values for the implantation samples were significantly smaller than those for the ICP sample, approaching 2. This indicates outstanding performance when employing the ion implantation process. Furthermore, due to the superior isolation effect in μLED (^{75}As), a lower ideality factor of 2.15 was exhibited in this study. However, this damage is difficult to observe in the implant process when the implant energy below 50 keV and the dosage below 1×10^{15}/cm^2[17]. Generally, heavy ion implants will more easily damage materials, including the n-GaN layer, leading to higher series resistance. In summary, a lower current was observed in μLED (^{75}As) than in μLED (^{40}Ar) at the same voltage. Overall, the device fabricated by ion implantation exhibited better electrical performance than that using ICP dry etching. To further elucidate the impact of R_s and R_p on μLED performance, the optical properties will be discussed in the next section.

Despite the electrical performance, the corresponding relationship with photoelectric properties is also important in the μLED study. Following this, light output power (LOP) was measured using integrating sphere systems and plotted in Fig. 4a. As the injection current increases from 0.1 to 30 mA, the LOP of the μLED (^{40}Ar) sample rises quickly from 0.023 to 4.77 mW. Similarly, the LOP of μLED (^{75}As) increased from 0.019 to 4.26 mW. In contrast, the μLED (ICP)

Table 2 Resistance, ideality factors, and peak EQE of three μLED samples in this study

Samples	R_d (@3V) (kΩ)	R_s (@3 to 4 V) (Ω)	R_p (@0.5 to 1.5 V)	Ideality factor	peak EQE (%)
μLED (As)	3.10	109.2	20.7 GΩ	2.15	9.82
μLED (Ar)	0.85	89.4	11.7 GΩ	2.21	11.03
μLED (ICP)	1.27	108.6	3.23 μΩ	11.89	8.67

sample exhibited the worst LOP, ranging from 0.011 to 3.53 mW. Despite the ability of the μLED (ICP) sample to emit from the sidewall, it still showed lower LOP compared to the other samples. The wall plug efficiency (WPE) of the three samples was also presented in the inset of Fig. 4a. Due to lower R_d and R_s, the highest WPE was observed in μLED (^{40}Ar) with a value of 10.66%. This result indicates that the value of R_s is more important than R_p in the operation of μLEDs, owing to the small emission area generating higher current density in the μLED device. A lower R_s will improve electrical-optical transferring efficiency. Meanwhile, the EQE was also calculated and plotted in Fig. 4b. The values of the peak EQE of the three samples are listed in Table 2, which were 9.82%, 11.03%, and 8.67% in μLED (^{75}As), μLED (^{40}Ar), and μLED (ICP), respectively. Due to higher LOP and WPE, it can be observed that the highest values of peak EQE occurred in the μLED (^{40}Ar) sample. Recently, a new approach was used to improving the efficiency of GaN-based micro-LEDs with full-M-sided hexagonal mesa combinaed with the treatment of TMAH solution. The corresponding EQE_{max} was about 10% [27]. Abviously, ^{40}Ar ion implantation can enhance electrical and optical properties and minimizing sidewall damage of μLEDs. Moreover, the EQE droop efficiency is also shown in the inset of Fig. 4b. A higher EQE decay ratio of 52% occurs in μLED (ICP), declining more than half of the peak EQE in this sample. The lower EQE of μLEDs was related to more defects in the LED epilayers, which will form non-radiative recombination centers. The carriers will be trapped by those recombination centers as Shockley–Read–Hall (SRH) recombination, which suppresses radiative recombination behavior and further decreases EQE values. Therefore, the higher SRH effect significantly impacts the μLED (ICP) sample, resulting in the disappointing performance observed in μLED (ICP).

To compare the emission patterns between ion implant and ICP processes, light emission profiles were measured using ImageJ software, as shown in Fig. 5. Additionally, electroluminescence (EL) pictures were exhibited in the inset of Fig. 5. The three-by-three array emitted at an injection current of 0.5 mA (current density 55.6 A/cm^2), and the μLED (^{40}Ar) sample presented lower intensity in the channels between each chip in the array, as depicted in Fig. 5a. Conversely, a serious optical crosstalk issue was observed in μLED (ICP) in Fig. 5b. Despite being emitted by three chips, the emission intensity remained at the same value, caused by the light emitted from the mesa sidewall in the μLED (ICP) sample. However, the LOP of μLED (ICP) and μLED (Ar) were 0.12 mW and 0.15 mW, respectively, at an input current of 0.5 mA. This indicates that inhibiting the SRH non-radiative recombination can not only extract more light emission but also avoid the optical crosstalk issue in μLED devices.

4 Conclusion

In this study, we explored the fabrication and performance of 10 μm chip size μLEDs using ion implantation and dry etching techniques. The investigation focused on two ion sources, ^{75}As and ^{40}Ar, with an implantation energy of 40 keV, as modeled by SRIM simulations. The higher atomic mass of ^{75}As resulted in shallower ion penetration compared to ^{40}Ar, with peak distributions at 17 and 25 nm, respectively. To evaluate the effects of these ions, we

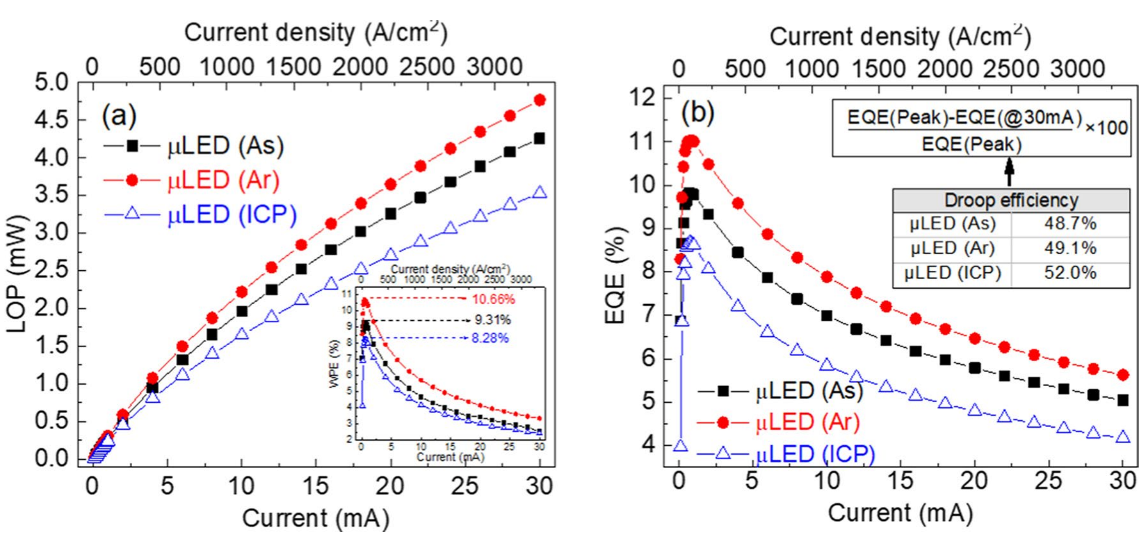

Fig. 4 **a** LOP and **b** EQE as the functions of current from 0.1 to 30 mA

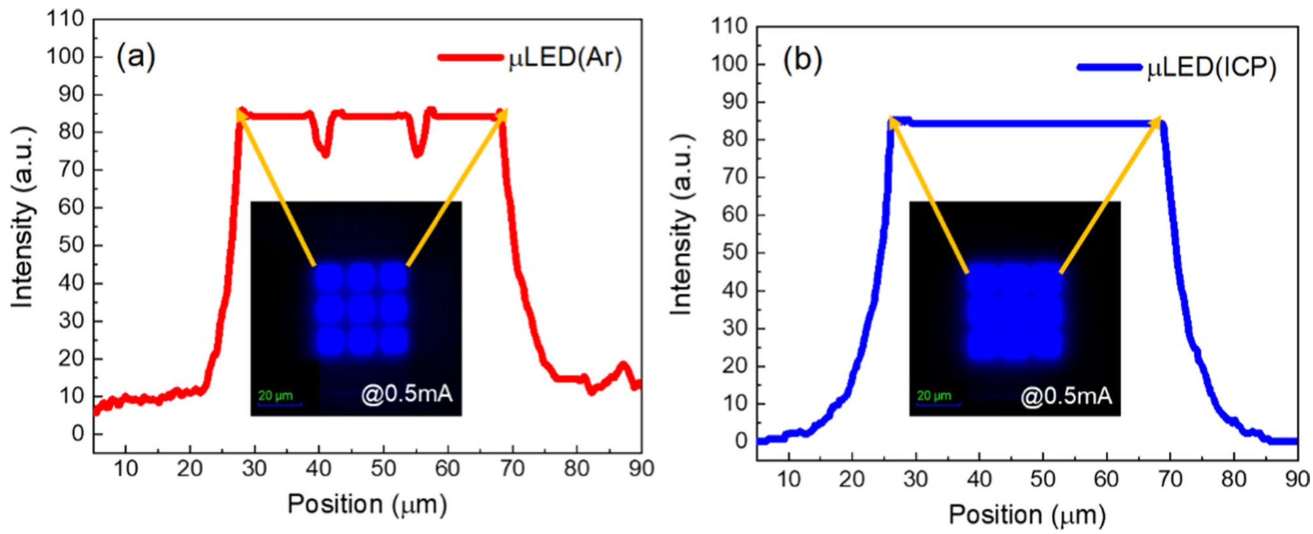

Fig. 5 Emission intensity profiles of **a** μLED (^{40}Ar) and **b** μLED (ICP) measured by ImageJ software

carefully adjusted the implant dosages to 4×10^{14} for ^{75}As and 8×10^{14} for ^{40}Ar, ensuring a fair comparison. Our results demonstrated that ion implantation significantly outperformed the dry etching process. The μLED (Ar) sample exhibited the highest IV slope, indicating the lowest Rd and Rs. This was evidenced by superior electrical properties, with a current of 1.14 mA at 3 V for μLED (Ar), compared to 0.97 mA for μLED (As) and 0.90 mA for μLED (ICP). The μLED (ICP) device showed notable leakage current and early turn-on issues, with a leakage current of 2.6 μA at – 5 V, significantly higher than the 1 nA observed in the implant samples. Optically, the μLED (^{40}Ar) demonstrated the highest light output power and WPE, achieving a peak WPE of 10.66%. The peak EQE was also highest in μLED (^{40}Ar) at 11.03%, significantly better than the μLED (ICP) at 8.67%. The study highlighted the detrimental impact of sidewall defects and non-radiative recombination centers, particularly in μLED (ICP) samples, which suffered from severe optical crosstalk and lower device performance. Overall, this study underscores the advantages of ion implantation over traditional dry etching in μLED fabrication, offering enhanced electrical and optical properties and minimizing sidewall damage. This process is crucial for developing high-efficiency, small-sized μLEDs, with potential applications in advanced display technologies.

Acknowledgements We thank the Nano Facility Center in National Yang Ming Chiao Tung University, Taiwan Semiconductor Institute Research, Industrial Technology Research Institute and Taiwan Instrument Research Institute and MA-Tek for facilities supporting.

Author contributions Y.H.H designed, process experiments and wrote the draft manuscript. S.H.L processed the μLED devices. D.S.W analysis the optical image data. R.H.H designed the experiments, analyzed and verified the data, and organized the paper. All authors read and approved the final version of the manuscript.

Funding This work was supported by the National Science and Technology Council (NSTC), Taiwan, R.O.C., under the grant nos. 113-2218-E-A49-019-MBK and113-2640-E-A49-008, 113-2923-E-A49-002-MY3, and by the Project of UI-UAAT Ministry of Education (MOE), Taiwan. This study was also supported by Science Park Emerging Technology Application Program, Taiwan, R.O.C. under the Grant No. B11202 and Industrial Technology Research Institute.

Data availability Data is provided within the manuscript.

Declarations

Competing interests The authors declare no competing interests.

References

1. Zhang K, Liu Y, Kwok HS, Liu Z. Investigation of electrical properties and reliability of GaN-based micro-LEDs. Nanomaterials. 2020;10(4):689. https://doi.org/10.3390/nano10040689.
2. Ding K, Avrutin V, Izyumskaya N, Özgür Ü, Morkoç H. Micro-LEDs, a manufacturability perspective. Appl Sci. 2019;9(6):1206. https://doi.org/10.3390/app9061206.
3. Liu Z, Zhang K, Liu Y, Yan S, Kwok H, Deen J, Sun X. Fully multi-functional GaN-based micro-LEDs for 2500 PPI micro-displays, temperature sensing, light energy harvesting, and light detection. In: 2018 IEEE Int. electron devices meeting (IEDM), IEEE, Piscataway, NJ; 2018. pp. 38.1.1–38.1.4.
4. Liu Z, Lin CH, Hyun BR, Sher CW, Lv Z, Luo B, Jiang F, Wu T, Ho CH, Kuo HC, He JH. Micro-lightemitting diodes with quantum dots in display technology. Light Sci Appl. 2020;9(1):83. https://doi.org/10.1038/s41377-020-0268-1.
5. Tian PF, McKendry JJD, Gu ED, Chen ZZ, Sun YJ, Zhang GY, Dawson MD, Liu R. Fabrication, characterization and applications of flexible vertical InGaN micro-light emitting diode arrays. Opt Express. 2016;24(1):699–707. https://doi.org/10.1364/OE.24.000699.
6. Huang YG, Hsiang EL, Deng MY, Wu ST. Mini-LED, Micro-LED and OLED displays: present status and future perspectives. Light Sci Appl. 2020;9(1):105. https://doi.org/10.1038/s41377-020-0341-9.
7. Zhou XJ, Tian PF, Sher CW, Wu J, Liu HZ, Liu R, Kuo HC. Growth, transfer printing and colour conversion techniques towards full-colour micro-LED display. Prog Quant Electron. 2020;71: 100263. https://doi.org/10.1016/j.pquantelec.2020.100263.
8. Bulashevich KA, Karpov SY. Impact of surface recombination on efficiency of III-nitride light-emitting diodes. Phys Status Solidi RRL. 2016;10(6):480–4. https://doi.org/10.1002/pssr.201600059.
9. Boussadi Y, Rochat N, Barnes JP, Bakir BB, Ferrandis P, Masenelli B, Licitra C. Investigation of sidewall damage induced by reactive ion etching on AlGaInP MESA for micro-LED application. J Lumi. 2021;234: 117937. https://doi.org/10.1016/j.jlumin.2021.117937.
10. Tian P, McKendry JJ, Gong Z, Guilhabert B, Watson IM, Gu E, Chen Z, Zhang G, Dawson MD. Size-dependent efficiency and efficiency droop of blue InGaN micro-light emitting diodes. Appl Phys Lett. 2012;101(23): 231110. https://doi.org/10.1063/1.4769835.
11. Jiang F, Hyun BR, Zhang Y, Liu Z. Role of intrinsic surface states in efficiency attenuation of gan-based micro-light-emitting-diodes. Phys Status Solidi. 2020;15(2):2000487. https://doi.org/10.1002/pssr.202000487.
12. Anwar AR, Sajjad MT, Johar MA, Hernández-Gutiérrez CA, Usman M, Lepkowski SP. Recent progress in micro-LED-based display technologies. Laser Photon Rev. 2022;16(6):2100427. https://doi.org/10.1002/lpor.202100427.
13. Chang C, Li H, Shih Y, Lu T. Manipulation of nanoscale V-pits to optimize internal quantum efficiency of InGaN multiple quantum wells. Appl Phys Lett. 2015;106(9): 091104. https://doi.org/10.1063/1.4914116.
14. Wong MS, Lee C, Myers DJ, Hwang D, Kearns JA, Li T, Speck JS, Nakamura S, DenBaars SP. Size-independent peak efficiency of III-nitride micro-light-emitting-diodes using chemical treatment and sidewall passivation. Appl Phys Exp. 2019;12: 097004. https://doi.org/10.7567/1882-0786/ab3949.
15. Park J-H, Pristovsek M, Cai W, Cheong H, Kumabe T, Lee D-S, Seong T-Y, Amano H. Interplay of sidewall damage and light extraction efficiency of micro-LEDs. Opt Lett. 2022;2022(47):2250–3. https://doi.org/10.1364/OL.456993.
16. Hsu YH, Hsu YC, Lin CC, Lin YH, Wuu DS, Kuo HC, Samukawa S, Horng RH. Performance improvement of blue light micro-light emitting diodes (<20 μm) by neutral beam etching process. Mater Today Adv. 2024;22:100496. https://doi.org/10.1016/j.mtadv.2024.100496.
17. Yin R, Li C, Zhang B, Wang J, Fu Y, Wen CP, Hao Y, Shen B, Wang M. Physical mechanism of field modulation effects in ion implanted edge termination of vertical GaN Schottky barrier diodes. Fundam Res. 2022;2(4):629–34. https://doi.org/10.1016/j.fmre.2021.11.027.
18. Zhuang Z, Iida D, Velazquez-Rizo M, Ohkawa K. Ultra-small InGaN green micro-light-emitting diodes fabricated by selective passivation of p-GaN. Optics Lett. 2021;46(20):5092–5. https://doi.org/10.1364/OL.438009.
19. Park J, Choi JH, Kong K, Han JH, Park JH, Kim N, Lee E, Kim D, Kim J, Chung D, Jun S, Kim M, Yoon E, Shin J, Hwang S. Electrically driven midsubmicrometre pixelation of InGaN micro-light-emitting diode displays for augmented-reality glasses. Nat Photon. 2021;15(6):449–55. https://doi.org/10.1038/s41566-021-00783-1.
20. Noor Elahi AM, Xu J. Electrical and optical modeling of gap-free III-nitride micro-LED arrays. AIP Adv. 2020;10(10):105028. https://doi.org/10.1063/5.0027809.
21. Slawinska J, Muziol G, Siekacz M, Turski H, Hajdel M, Zak M, Feduniewicz-Zmuda A, Staszczak G, Skierbiszewski C. Ion implantation of tunnel junction as a method for defining the aperture of III-nitride-based micro-light-emitting diodes. Optics Exp. 2022;30(15):27004–14. https://doi.org/10.1364/OE.458950.
22. Ye JY, Peng YY, Luo CL, Wang HA, Zhou XT, Guo TL, Sun J, Yan Q, Zhang YA, Wu CY. Pixelation of GaN based Micro-LED arrays by tailoring injection energy and dose of fluorine ion implantation. J Lumi. 2023;261: 119903. https://doi.org/10.1016/j.jlumin.2023.119903.
23. Liu SG, Han SC, Xu CC, Xu HW, Wang XY, Wang D, Zhu YK. Enhanced photoelectric performance of GaN-based Micro-LEDs by ion implantation. Opt Mater. 2021;121: 111579. https://doi.org/10.1016/j.optmat.2021.111579.
24. Xu F, Gao CH, Fan YM, Chen P, Zhang BS. Enhanced performance of vertical-structured InGaN micro-pixelated light-emitting-diode array fabricated using an ion implantation process. Optics Lett. 2019;44(18):4562–5. https://doi.org/10.1364/OL.44.004562.
25. Xu F, Tan Y, Xie ZL, Zhang BS. Implantation energy- and size-dependent light output of enhanced-efficiency micro-LED arrays fabricated by ion implantation. Optics Exp. 2021;29(5):7757–66. https://doi.org/10.1364/OE.421272.
26. Hsu YH, Wang CH, Lin XD, Lin YH, Wuu DS, Horng RH. Improved electrical properties of micro light-emitting diode displays by ion implantation technology. Discover Nano. 2023;18(1):48. https://doi.org/10.1186/s11671-023-03819-3.
27. Zhang P, Hua H, Gu Y, Gong Y, Huang M, Yang W, Zhu J, Long S, Lu S. External quantum efficiency enhancement of GaN-based blue LEDs by treating their full-M-sided hexagonal mesa with TMAH solution. Optics Lett. 2024;49(17):4954–7. https://doi.org/10.1364/OL.533252.